JOURNAL OF PROPULSION AND POWER
Vol. 24, No. 2, March–April 2008

Aluminum-Rich Al–MoO_3 Nanocomposite Powders Prepared by Arrested Reactive Milling

Swati M. Umbrajkar,* Soumitri Seshadri,† Mirko Schoenitz,‡
Vern K. Hoffmann,§ and Edward L. Dreizin¶
New Jersey Institute of Technology, Newark, New Jersey 07402

DOI: 10.2514/1.31762

Fuel-rich Al–MoO_3 nanocomposites were prepared using arrested reactive milling. Powder composition was varied from 4Al + MoO_3 to 16Al + MoO_3. Powders were evaluated using electron microscopy, thermal analysis, x-ray diffraction, heated-filament-ignition experiments, and constant-volume-explosion experiments. Uniform mixing of MoO_3 nanodomains in the aluminum matrix was achieved for all prepared powders. Multiple and overlapping exothermic processes were observed to start when the nanocomposite powders were heated to only about 350 K. In heated-filament experiments, all nanocomposite powders ignited at temperatures well below the aluminum melting point. Ignition temperatures for these powders were estimated for the higher heating rates that are typical of fuel–air explosions. Constant-volume-explosion experiments indicated that flame propagation in aerosols of nanocomposite thermite powders in air is much faster than that in pure aluminum aerosols. The energy release, normalized per unit mass of aluminum, was higher for the nanocomposite materials with bulk compositions 4Al + MoO_3 and 8Al + MoO_3 and lower for pure aluminum and for the 16Al + MoO_3 nanocomposite sample. The reaction rate was the highest for the 8Al + MoO_3 nanocomposite powder. The combustion efficiency inferred from the measured pressure traces correlated well with the phase compositions of the analyzed condensed combustion products.

I. Introduction

NANOSTRUCTURED materials are receiving significant attention in fields from electronics to the pharmaceutical industry due to their novel and unique properties. Reactive nanocomposite powders exploiting the exothermic nature of thermite reactions [1,2] have attracted a great deal of interest for use in ordnance applications. Different types of reactive nanocomposites have been prepared, including mixed nanopowders [also called metastable intermolecular composites (MIC)] [3–9], porous nanocomposites produced by sol-gel synthesis [9–12], self-assembled composites [13], multilayer nanofoils [14–16], and dense nanocomposite powders produced by arrested reactive milling (ARM) [17–21]. Despite different preparative techniques and material types, the common approach is to increase the interface area available for heterogeneous reaction between solid fuel and oxidizer components. In this project, fully dense reactive nanocomposite powders were prepared using ARM. ARM is derived from reactive milling, in which a self-sustaining reaction is triggered mechanically after a certain time when a blend of powders capable of a sufficiently exothermic reaction is ball-milled [22]. In ARM, metastable nanocomposites with high energy densities are formed as a result of arresting (or stopping) the milling process before the initiation of such a self-sustaining reaction. Initial results showed that micron-sized nanocomposite powders prepared by ARM have a high reactivity, comparable with that of chemically similar mixed nanopowder compositions, and they offer potential advantages in handling, maximum packing density, and cost. For many applications of energetic formulations, an external oxidizer (e.g., oxygen from air or from a propellant formulation) will be used and thus the stoichiometric thermite compositions are of limited interest. For such applications, it is proposed to develop off-stoichiometric, metal-rich reactive nanocomposites. This project deals with the corresponding Al–MoO_3 compositions. One objective of this work is to determine the maximum aluminum concentration that can be used for the nanocomposite to remain sufficiently reactive to warrant its practical applications. The project includes preparation of several nanocomposite powders and characterization of their morphologies and reactivities. X-ray diffraction, electron microscopy, and thermal analysis were used to characterize the prepared materials. In addition, ignition tests using an electrically heated filament and constant-volume-explosion experiments were also conducted.

II. Material Preparation

A shaker mill (8000 series by Spex CertiPrep) was employed in this research. Flat-ended steel vials were used with steel milling media of 5-mm diameter. Starting blends were prepared in off-stoichiometric proportions from powders of elemental aluminum (99% pure, −325 mesh by Alfa Aesar) and molybdenum trioxide MoO_3 (99.95% pure, by Alfa Aesar). Preparation was carried out in an argon environment using 5-g powder batches with different Al/MoO_3 ratios, and 4 ml of hexane (C_6H_{14}) was added as a process control agent (PCA) to inhibit both cold welding and partial reaction during milling. The process temperature was monitored using a thermistor attached to the side of the milling vial and connected to a digital data logger. The instant of reaction was marked by a sharp rise in the vial temperature. The stoichiometric composition requires 2 mol of Al, corresponding to each mole of MoO_3. Preliminary experiments in which the samples were milled dry established that the self-sustaining reaction was mechanically triggered during milling for the blends with up to 10 moles of Al per mole of MoO_3. Typically, the reaction would occur within the first few minutes of dry milling. It was also observed that adding hexane as a process control agent avoided the rapid triggering of exothermic reaction and obtained uniform nanocomposite powders. For further experiments, four samples were prepared with aluminum concentrations of 4, 8, 12, and 16 mol per mole of MoO_3. Wet milling (with hexane as the

Presented as Paper 294 at the 45th AIAA Aerospace Sciences Meeting and Exhibit, Reno, NV, 8–11 January 2007; received 25 April 2007; accepted for publication 10 September 2007.

*Graduate Student, Department of Mechanical Engineering. Member AIAA.
†Undergraduate Student, Department of Mechanical Engineering.
‡Assistant Research Professor, Department of Mechanical Engineering. Member AIAA.
§Senior Research Engineer, Department of Mechanical Engineering.
¶Professor, Department of Chemical Engineering. Senior Member AIAA.

PCA) and a constant milling time of 30 min were used to achieve a similar degree of structural and compositional refinement for all samples. After milling, the samples were collected, dried in vacuum, and stored in an argon-filled glove box.

III. Sample Characterization

Morphology and composition of the nanocomposites were examined on a LEO 1530 field emission scanning electron microscope (SEM) operated at 10 kV. The nanocomposite samples were embedded in epoxy and cross-sectioned for examination. The phase composition was determined for each nanocomposite by x-ray diffraction (XRD). The XRD was performed on a Phillips X'pert MRD powder diffractometer operated at 45 kV and 45 mA using Cu-K_α radiation ($\lambda = 1.5438$ Å).

Temperature-dependent structural transformations were determined by differential scanning calorimetry (DSC) using a Netzsch simultaneous thermal analyzer STA409 PC. Alumina pans were used and the furnace was flushed with argon at approximately 50 ml/min. DSC traces were recorded with heating rates varying from 1 to 40 K/min. The samples were heated from room temperature to 1200 K, held at 1200 K for 30 min, and then cooled to room temperature. Without disturbing the experiment, the samples were then heated to 1200 K for the second time to record the baseline signal. The temperature was accurate within ± 1 K.

IV. Ignition and Constant-Volume-Explosion Experiments

Ignition of the prepared powders was studied at heating rates ranging approximately from 2000 to 20,000 K/s. The reactive powder was coated on an electrically heated Nichrome® filament. The value of the dc voltage applied to the filament determined the experimental heating rate. The temperature of the uncoated portion of the filament was monitored with an infrared pyrometer. Light emission from the powder coating was detected by a separate photosensor. A sharp onset of the light emission was taken as evidence of ignition and the temperature recorded for that instant was considered as the measured ignition temperature. The setup is described in detail elsewhere [23,24].

Combustion of the prepared nanocomposite powders was studied using constant-volume-explosion (CVE) experiments. A 9.2-liter explosion vessel was used. The vessel was initially evacuated. A short gas blast delivered from a high-pressure reservoir through a nozzle with multiple small openings introduced powder into the vessel and simultaneously established the initial gas environment and pressure. After a short delay, aerosolized powder was ignited by a heated filament placed in the center of the vessel and the pressure was monitored using a pressure transducer. Experiments were performed in a mixture of 22.5% O_2 and 77.5% N_2. The ratio of the maximum explosion pressure to the initial pressure before ignition and the maximum rate of pressure rise were used to assess the energy released in each explosion and the rate of combustion, respectively. Condensed combustion products were collected after each experiment for subsequent analysis. In addition to the nanocomposite powders, a spherical aluminum powder (by Atlantic Equipment Engineers, 99.9% pure, with a nominal size of 1–5 μm) was used in these experiments for reference. This reference sample was selected based on earlier experiments [25] in which it was found to give the highest explosion pressures and rates of pressure rise among several different aluminum powders. A detailed description of the experimental setup and procedure is available elsewhere [26,27]. The experimental methodology is based on a technique developed by the U.S. Bureau of Mines for characterization of the explosibility of various dusts [28,29]. In the preliminary tests using the experimental conditions described in [27], it was found that some of the nanocomposite powders ignited upon entering the explosion vessel with the gas blast. To avoid such uncontrolled ignition, the gas blast duration was increased and the pressure in the reservoir was reduced. The final operating parameters were as follows: gas blast duration of 500 ms, reservoir pressure of 2.45 atm, initial pressure in the explosion vessel before ignition of 1 atm, and delay between the gas blast and ignition of 300 ms.

V. Results and Discussion

A. Particle Sizes

Particle size distributions of the nanocomposite powders were determined by low angle laser light scattering using a Coulter LS 230 enhanced laser diffraction particle size analyzer. Measurements required suspension of small quantities of powder in deionized water. Figure 1 shows the particle size distribution (PSD) of the as-milled nanocomposite powders, as well as of the spherical aluminum powder used for reference in the CVE experiments. It was observed that the particle size increased with increasing aluminum concentration. For the results of CVE experiments to be useful in terms of identifying the effect of material composition, the particle sizes for powders of different materials must be close. The PSD of the nanocomposite sample with bulk composition $4Al + MoO_3$ was found to be reasonably close to that of the reference aluminum powder. However, for the nanocomposite samples with higher aluminum concentrations, the particles were noticeably coarser when compared with the reference aluminum. Therefore, the preceding nanocomposite powders were size-classified using a 450 mesh sieve. Figure 2 shows the PSD of the size-classified powders used in CVE experiments (along with as-prepared $4Al + MoO_3$ and spherical Al powders). The particle sizes for the sieved powders were still noticeably coarser than for the reference aluminum, which should be considered when interpreting the results of the CVE experiments. In the future, if necessary, particle sizes can be reduced using milling at cryogenic temperatures or other techniques. Likewise, although examination by SEM suggests that the powders are compositionally homogeneous across size fractions, this should be confirmed by explicit measurements of the classified powders before use in any practical application.

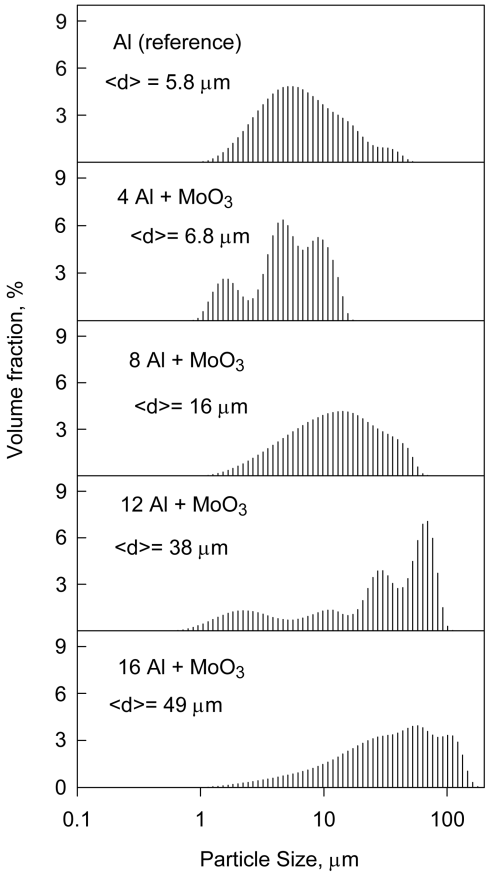

Fig. 1 Particle size distribution of the as-milled nanocomposite powders. The size distribution is also shown for the aluminum powder used for reference constant-volume-explosion experiments.

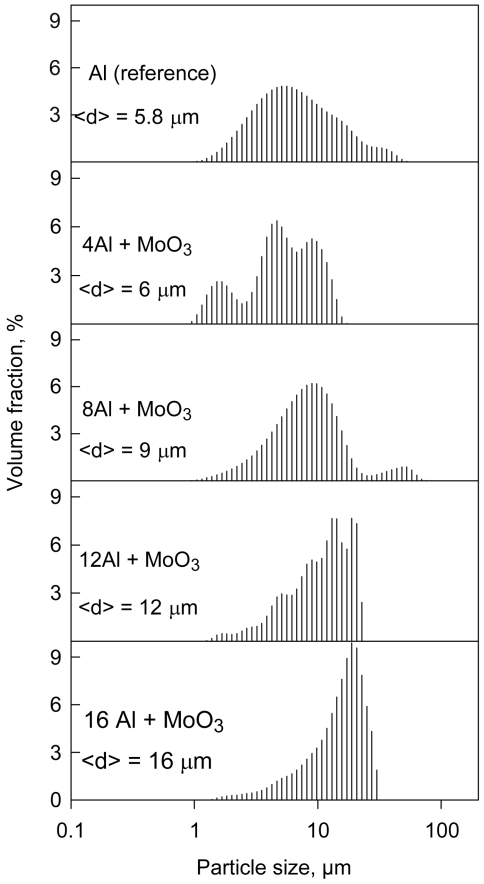

Fig. 2 Particle size distribution of the nanocomposite powders after sieving. The size distribution is also shown for the aluminum powder used for reference constant-volume-explosion experiments.

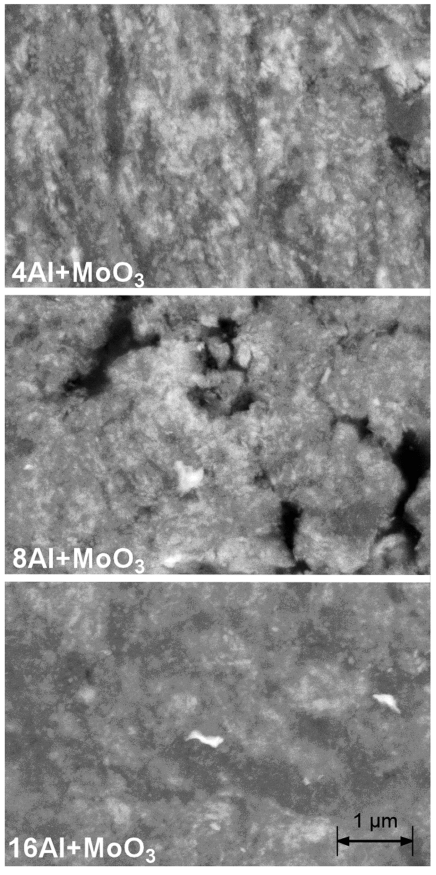

Fig. 3 Back-scattered electron SEM images of Al–MoO_3 nanocomposites with varying concentrations of Al.

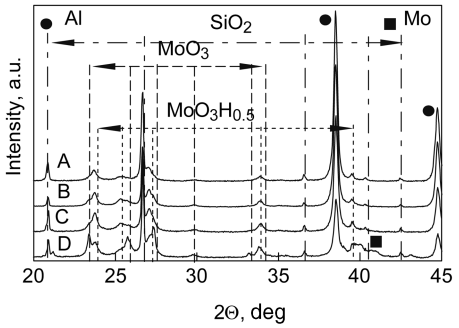

Fig. 4 XRD patterns of samples with varying concentrations of Al.

B. Morphology of Nanocomposite Powders

Back-scattered SEM images of cross-sectioned samples of the Al–MoO_3 nanocomposites with different bulk compositions are shown in Fig. 3. The dark background is epoxy used for embedding the sample, the gray areas indicate aluminum matrix, and the light inclusions indicate MoO_3. Al and MoO_3 are sandwiched together and form a fully dense material with a highly developed reactive interface. For all the prepared compositions, the elongated nanosized MoO_3 inclusions were uniformly distributed in the Al matrix. No significant change in the size of MoO_3 inclusions as a function of the bulk material composition was observed. In some samples, the presence of the fully reacted phases [e.g., Mo (very bright, white component) and Al_2O_3 (dark, uniform component)] was detected, indicating that a chemical reaction was initiated during milling, although it did not propagate over the entire sample. Most of the reacted phases were observed for the $4Al + MoO_3$ sample. This reaction is undesirable and should be avoided for optimized conditions.

C. Phase Compositions

Figure 4 shows the XRD patterns of the nanocomposites prepared with different aluminum concentrations (note that SiO_2 peaks appear because quartz powder was added as an internal standard for the XRD measurements). As expected, the intensities of Al peaks decrease and MoO_3 peaks increase with reduced aluminum concentration. The aluminum peak at around 45 deg is somewhat distorted because of an overlap with a peak of Fe occurring nearly at the same angle. Iron in the XRD patterns indicates minor contamination of the sample by the milling media. Peaks of $MoO_3H_{0.5}$ are observed for all samples. The intensity of these peaks changes only slightly with sample composition. A possible source of hydrogen could be hexane used as a surface control agent. Presence of metallic Mo was also noticed in the XRD patterns. Metallic Mo indicates that the reaction between Al and MoO_3 was mechanically triggered during milling, but was not self-sustained. To assess the extent of this undesirable partial reaction, the XRD patterns were processed using the General Structure Analysis System (GSAS) whole-pattern-refinement software [30]. The relative amounts of Mo and MoO_3 phases were compared for all samples. The calculated mass ratio of Mo and MoO_3 as a function of bulk aluminum concentration is shown in Fig. 5. It is clear that the reaction was most significant for the $4Al + MoO_3$ sample. The crystallite size of aluminum was also evaluated from the refinement and was estimated to vary in the range of 35–45 nm.

D. Reactions upon Heating

Figure 6 shows baseline-corrected DSC traces for the three nanocomposite samples with different bulk compositions heated to 1200 K at a rate of 2 K/ min. The heating was accompanied by several overlapping exothermic peaks occurring before the aluminum melting point, which is indicated by a vertical dotted

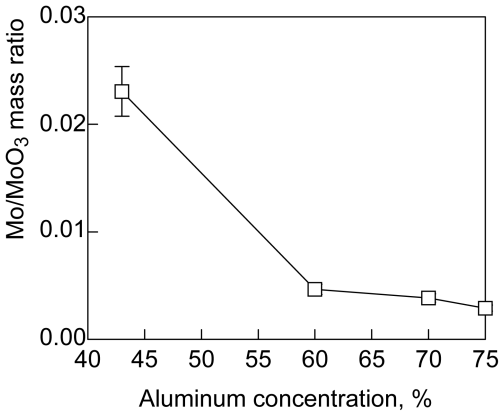

Fig. 5 Mass ratio of Mo/MoO_3 phases calculated using experimental XRD traces and whole-pattern-refinement software [30] for samples with different aluminum concentrations.

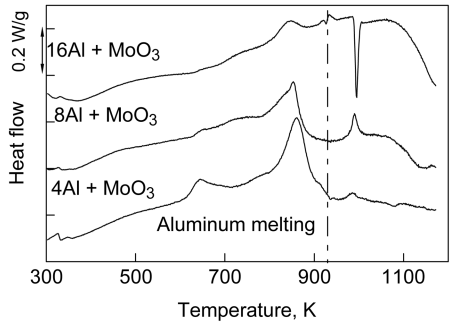

Fig. 6 Baseline-corrected DSC traces of nanocomposite powders recorded at 2 K/min.

line. For all samples, the first exothermic process starts at a temperature below 400 K. A broad exothermic hump was reproducibly observed between 350 and 500 K. This hump was followed by a weak exothermic peak between 600 and 750 K. A strong exothermic peak was observed to occur between 800 and 900 K. Additional weak and poorly resolved exothermic features were observed (e.g., around 700 and 900 K). An exothermic peak was also observed in the vicinity of 1000 K, above the melting point of Al. An endothermic peak indicating aluminum melting was not clearly detected for all samples, most likely because of overlap with exothermic features. A second strong endothermic peak was observed for the $16Al + MoO_3$ sample at 1000 K. This peak appears to indicate melting of $Al_{12}Mo$ and peritectic formation of Al_5Mo reported to occur around 1000 K [31]. For samples with lower concentration of aluminum, this endothermic peak was masked by an exothermic peak.

The kinetics of the observed exothermic reactions are of interest for both modeling ignition and predicting stability of the prepared nanocomposite powders. However, the quantitative analysis of such kinetics is not straightforward. An initial attempt was made to analyze the obtained DSC traces using an isoconversion approach [32]. It was found, however, that such analysis is not meaningful and that a detailed kinetic model needs to be developed instead. Development of such a model is outside the scope of this paper and will be addressed in future work. Additional details describing isoconversion data processing from the DSC experiments with metal-rich Al–MoO_3 nanocomposite powders are available elsewhere [32].

E. Ignition Temperatures

Figure 7 shows the ignition temperatures of the Al–MoO_3 nanocomposites as a function of heating rate. Each point represents the average of at least seven measurements taken at the same experimental conditions. The error bars show the standard deviations

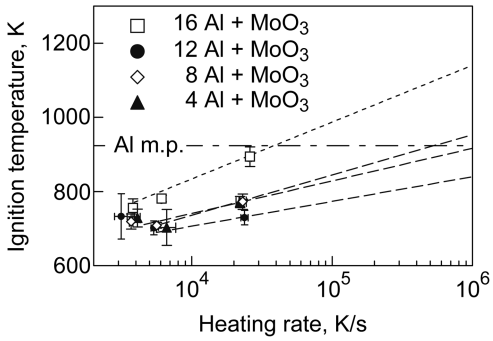

Fig. 7 Ignition temperatures of the nanocomposites at different heating rates.

obtained for each experimental data set. The aluminum melting point is shown for reference as a dotted line. Clearly, all samples ignited at temperatures well below the Al melting point. At the lowest heating rate used (around 2000–3000 K/s), ignition occurred in about the same temperature range of 720–750 K for all the samples.

For the sample with bulk composition $16Al + MoO_3$, increased heating rates resulted in higher ignition temperatures, as expected for a thermally activated ignition process. If these particles were to be used in an explosive formulation, they would be subjected to much higher heating rates, on the order of 10^6 K/s. Therefore, for this specific composition, tentative extrapolation into this range would result in an ignition temperature of 1160 K, provided that the ignition mechanism remains unchanged. This exact number is rather speculative, but it illustrates the point that any computation of blast performance would need to take the variable ignition temperature into account.

For samples with lower concentrations of Al, an increase in the heating rate initially resulted in a small but reproducible decrease in the ignition temperature. Further increase in the heating rate resulted in the regular trend of increased ignition temperature. Note also that all three remaining samples ignited at very close temperatures for all heating rates. The trend observed in Fig. 7, based on the two higher heating rate experiments (neglecting the point at the lowest heating rate) combined for all three of these samples, suggests that the ignition temperature of these powders would increase to about 910 K at a practically relevant heating rate of 10^6 K/s. The unusual decrease in the ignition temperature observed for the three samples between the heating rates of approximately 2000 and 7000 K/s can be interpreted by assuming a change in the ignition mechanism occurring upon increase in the heating rate. In other words, it can be suggested that for these materials, different exothermic processes result in a thermal runaway when the samples are heated at different heating rates.

F. Combustion Experiments

The main goal of the CVE experiments was to compare the combustion performance of different reactive nanocomposite powders between one another and to compare their performance with that of a pure aluminum powder. Before the experiments, adiabatic flame temperatures and respective combustion-product compositions were determined for different materials using the NASA Chemical Equilibrium with Applications (CEA) code.** Calculations were performed for a constant-volume case, with the volume of the combustion chamber filled with a gas mixture of 22.5% O_2 and 77.5% N_2, selected to match the volume of the experimental explosion vessel of 9.2. liters. Predicted adiabatic flame temperatures for varied loads of different powders are shown in Fig. 8. The nanocomposite powders were represented by their respective bulk compositions of Al and MoO_3. The presence of small quantities of reaction products formed during milling was neglected.

**Data available online at http://www.grc.nasa.gov/WWW/CEAWeb [retrieved 21 January 2008].

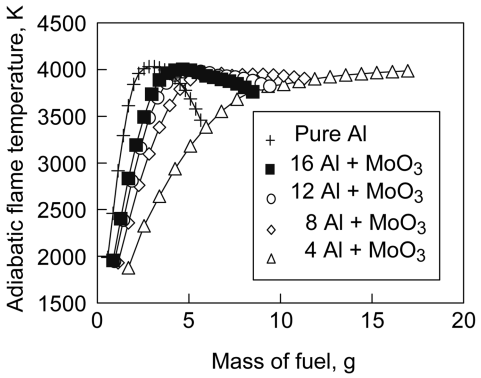

Fig. 8 Calculated adiabatic flame temperatures for the N_2/O_2 gas mixtures with a fixed O_2 concentration of 22.5% with Al and xAl + MoO_3 fuels.

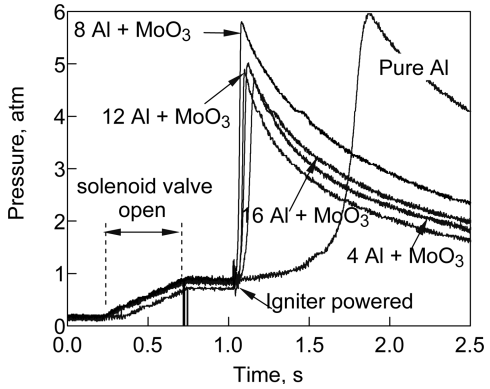

Fig. 9 Pressure traces of the Al and Al–MoO_3 nanocomposites with varying Al concentrations recorded during CVE.

For experiments with Al powder, the amount was selected that resulted in the highest predicted adiabatic flame temperature (i.e., 2.89 g). This case corresponded closely to a stoichiometric Al–air mixture. A similar choice could not be made for all the nanocomposite powders, because the increase of the mass of powder, which includes both Al fuel and MoO_3 oxidizer, can result in a continuous increase in the flame temperature, as clearly seen for 4Al + MoO_3 (cf. Fig. 8). For nanocomposite powders with smaller aluminum concentrations, the amounts of powder that correspond to the maximum temperatures increase significantly compared with those of pure Al. Therefore, using amounts of nanocomposite powders that correspond to the maximum predicted adiabatic flame temperatures was impractical. Instead, the amounts of nanocomposite powder were selected to match the volume of the reference aluminum sample. In other words, the volume of powder used in the CVE experiments remained constant for all materials. The powder amounts used in these experiments for different materials are shown in Table 1. Also shown in Table 1 is the mass of pure Al contained in each experimental charge.

Characteristic CVE pressure traces for different materials are shown in Fig. 9. The pressure trace recorded in an experiment with pure Al powder indicates a significant delay between the instant the igniter was triggered and the time when a substantial increase in pressure was observed. However, all nanocomposite powders combusted without any noticeable delay, an indication of their higher reactivity than with aluminum. To a first approximation, the ratio of the maximum CVE pressure $P_{\max}$ over the initial pressure in the vessel is proportional to the flame temperature. The maximum pressures are practically identical for pure Al and for the 8Al + MoO_3 nanocomposite powder. The maximum pressures are somewhat lower for other nanocomposite samples.

A crude evaluation of the heat release produced in CVE experiments can be made assuming that the released heat ΔQ is generally proportional to the temperature increase in the vessel:

$$\Delta Q \cong \rho v C_v (T_{\max} - T_{\text{ini}})$$

where ρ and v are, respectively, the density and volume of the mixture; C_v is the specific heat at constant volume; and T_{ini} is the initial temperature (i.e., room temperature). Assuming further that the behavior of the heated combustion products is similar to that of an ideal gas, one can write that

Table 1 Amounts of powder used in CVE tests and the amount of pure Al contained in each charge

Fuel	Powder load, g	Amount of aluminum, g
4Al + MoO_3	3.81	1.64
8Al + MoO_3	3.48	2.09
12Al + MoO_3	3.32	2.29
16Al + MoO_3	3.23	2.42
Al	2.89	2.89

$$T_{\max} \approx T_{\text{ini}} \frac{P_{\max}}{P_{\text{ini}}}$$

Therefore, the heat release normalized by the amount of aluminum contained in each of the tested powders can be compared based on the following estimate:

$$\frac{\Delta Q}{m_{\text{Al}}} \sim \frac{T_{\text{ini}}}{m_{\text{Al}}} \left(\frac{P_{\max}}{P_{\text{ini}}} - 1 \right)$$

The left-hand side of the preceding equation is plotted in Fig. 10 as a function of the material composition. The amount of aluminum is taken from Table 1. Based on Fig. 10, it appears that for both 4Al + MoO_3 and 8Al + MoO_3 nanocomposite powders, the normalized energy release was nearly the same and much higher than that for pure aluminum powder. However, with increased aluminum concentration, the energy release quickly approaches that of pure aluminum, indicating reduced combustion efficiency. Most likely, the relatively sharp drop in combustion efficiency is associated with the larger particle size for the nanocomposite powders with higher aluminum concentrations (cf. Figs. 1 and 2). Thus, reducing particle sizes for such materials (e.g., by using milling at cryogenic temperatures) may prove to be a promising approach.

The combustion rate of the powders is evaluated from the maximum rate of pressure rise, $\mathrm{d}p/\mathrm{d}t_{\max}$. In CVE experiments, this is proportional to the burn rate [33]. The $\mathrm{d}p/\mathrm{d}t_{\max}$ was calculated by differentiating the recorded pressure traces. The results in terms of the maximum rates of pressure rise plotted as a function of the material composition are shown in Fig. 11. The value of $\mathrm{d}p/\mathrm{d}t_{\max}$, and thus the burn rate of the 8Al + MoO_3 sample, was the highest. The burn rates for all prepared nanocomposite powders exceed that of pure aluminum.

The combustion products were collected and their composition was investigated using x-ray powder diffraction. The resulting XRD

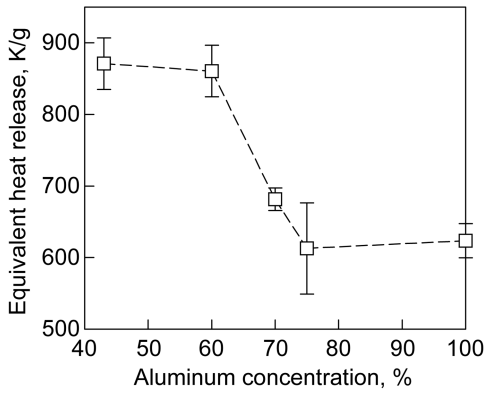

Fig. 10 Equivalent heat release normalized per mass of aluminum for different powder compositions.

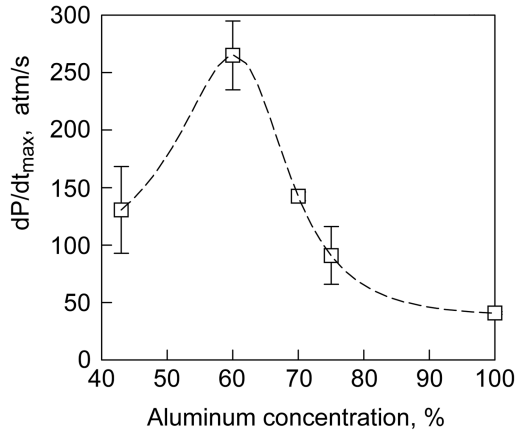

Fig. 11 Maximum rates of pressure rise measured in CVE experiments, dp/dt_{max}, as a function of the powder composition. The dashed line indicates a polynomial interpolation to fit the data points.

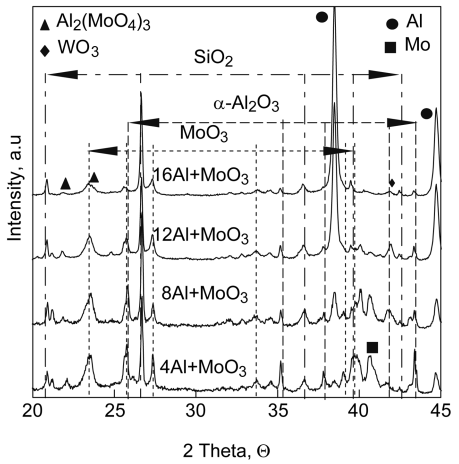

Fig. 12 XRD patterns of CVE combustion products of different nanocomposite powders.

patterns are shown in Fig. 12. As in the as-milled powders, quartz was added to the samples as an internal standard. In agreement with the combustion efficiency of aluminum already discussed (cf. Fig. 10), the peaks of metallic Al indicating unburned metal are stronger for the products of powders with higher initial aluminum concentrations. The peaks of WO_3 are most likely due to the presence of burned fragments of the igniter wire made of tungsten.

A more quantitative estimate of the reaction completeness can be obtained by comparing the intensity ratio of a characteristic Al_2O_3 peak with that of a characteristic Al peak. This ratio as a function of the material composition (including the results for pure Al powder not presented in Fig. 12) is shown in Fig. 13. As expected, the reaction is most complete (the highest ratio of Al_2O_3/Al peak intensity) for the lowest aluminum concentration in the nanocomposite powder. For the sample with bulk composition $16Al + MoO_3$, the reaction completeness is less than that of pure Al powder. Again, this can be explained by a substantial difference in the particle sizes (cf. Fig. 2). Even after sieving, the nanocomposite particles had an average particle size of 16 μm, compared with 6 μm for aluminum.

VI. Conclusions

Fuel-rich Al–MoO_3 nanocomposites with varying compositions were prepared. Uniform mixing of MoO_3 nanodomains in an Al matrix is achieved for all samples. The particle size of the nanocomposite powders increases with an increase in aluminum concentration. Thermal analysis showed that exothermic processes start when the nanocomposite powders are heated to only about

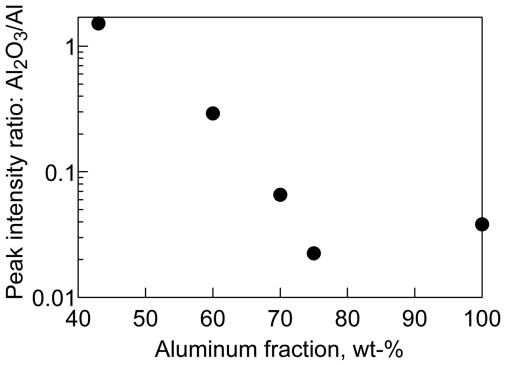

Fig. 13 Results of XRD analysis of combustion products collected in CVE experiments: intensity ratios for peaks of Al_2O_3 and Al.

350 K. Multiple and overlapping exothermic processes are observed and further work is needed to understand the reaction mechanisms in these materials. At heating rates varied in the range of 3000–30, 000 K/s, all nanocomposite powders ignite at temperatures well below the Al melting point. Ignition temperatures of samples containing 4, 8, and 12 mol of Al per mole of MoO_3 are similar and lower than those of the sample containing 16 mol of Al. It is noted that for the less-Al-rich samples, the ignition mechanism may change as the heating rate increases. Based on the current measurements, it is tentatively estimated that the nanocomposite powder with the bulk composition $16Al + MoO_3$ will ignite at about 1160 K when heated at a rate of 10^6 K/s, typically occurring in fuel–air explosions. The nanocomposite powders with lower aluminum concentrations are expected to ignite at an even lower temperature of about 910 K when heated at 10^6 K/s. Although these values remain to be refined in future research, it is recommended to incorporate the behavior shown here in any computations of propellant or explosive performance.

Constant-volume-explosion experiments indicate that the flames produced by nanocomposite thermite powders in air propagate much faster than those produced by pure Al powder. The maximum rate of pressure rise indicative of the highest burn rate was measured for the $8Al + MoO_3$ nanocomposite powder. Maximum reaction pressure indicative of the overall combustion energy is highest for pure Al, closely followed by that for $8Al + MoO_3$ and followed by those for the $12Al + MoO_3$ and $4Al + MoO_3$ nanocomposite powders. The reaction energy normalized per unit mass of aluminum is the highest for nanocomposite materials with bulk compositions $4Al + MoO_3$ and $8Al + MoO_3$ and lowest for pure Al and the $16Al + MoO_3$ nanocomposite sample. This reduced efficiency of combustion inferred from the measured pressure traces correlates with the analyzed combustion products containing greater amounts of unreacted aluminum. It is suggested that a reduced efficiency of combustion for very aluminum-rich nanocomposite powders is explained by relatively coarse particle sizes obtained for these materials.

Acknowledgment

This work was funded by the Defense Threat Reduction Agency award DAAE30-1-9-0080.

References

[1] Wang, L. L., Munir, Z. A., and Maximov, Y. M., "Thermite Reactions: Their Utilization in the Synthesis and Processing of Materials," *Journal of Materials Science*, Vol. 28, No. 14, 1993, pp. 3693–3708. doi:10.1007/BF00353167

[2] Chernenko, E. V., Afanas'eva, L. F., Lebedeva, V. A., and Rozenband, V. I., "Inflammability of Mixtures of Metal Oxides with Aluminum," *Combustion, Explosion, and Shock Waves*, Vol. 24, No. 6, 1988, pp. 639–646. doi:10.1007/BF00740402

[3] Son, S. F., Asay, B. W., Busse, J. R., Jorgensen, B. S., Bockmon, B., and Pantoya, M., "Reaction Propagation Physics of Al/MoO_3 Nano-

composite Thermites," *Twenty-Eighth International Pyrotechnics Seminar*, International Pyrotechnics Society, Fort Collins, CO, 4–9 Nov. 2001, pp. 833–843.

[4] Son, S. F., "Performance and Characterization of Nanoenergetic Materials at Los Alamos," *Material Research Society Symposium Proceedings*, Vol. 800, Materials Research Society, Warrendale, PA, 2004, pp. AA5.2.1–AA5.2.12.

[5] Moore, D. S., Son, S. F., and Asay, B. W., "Time-Resolved Spectral Emission of Deflagrating Nano-Al and Nano-MoO_3 Metastable Interstitial Composites," *Propellants, Explosives, Pyrotechnics*, Vol. 29, No. 2, 2004, pp. 106–111. doi:10.1002/prep.200400038

[6] Granier, J. J., and Pantoya, M. L., "Laser Ignition of Nanocomposite Thermites," *Combustion and Flame*, Vol. 138, No. 4, 2004, pp. 373–383. doi:10.1016/j.combustflame.2004.05.006

[7] Wilson, D. E., and Kim, K., "A Simplified Model for the Combustion of Al/MoO_3 Nanocomposite Thermites," 39th AIAA/ASME/SAE/ASEE Joint Propulsion Conference, Huntsville, AL, AIAA Paper 2003-4536, Hunstville, AL, 2003.

[8] Plantier, K. B., Pantoya, M. L., and Gash, A. E., "Combustion Wave Speeds of Nanocomposite Al/Fe_2O_3: the Effects of Fe_2O_3 Particle Synthesis Technique," *Combustion and Flame*, Vol. 140, No. 4, 2005, pp. 299–309. doi:10.1016/j.combustflame.2004.10.009

[9] Gash, A. E., Tillotson, T. M., Satcher, J. H., Hrubesh L. W., Jr., and Simpson. R. L., "New Sol-Gel Synthetic Route to Transition and Main-Group Metal Oxide Aerogels Using Inorganic Salt Precursors," *Journal of Non-Crystalline Solids*, Vol. 285, Nos. 1–3, 2001, pp. 22–28. doi:10.1016/S0022-3093(01)00427-6

[10] Tillotson, T. M., Gash, A. E., Simpson, R. L., , Satcher, J. H., and Poco, J. F., "Nanostructured Energetic Materials Using Sol-Gel Methodologies," *Journal of Non-Crystalline Solids*, Vol. 285, Nos. 1–3, 2001, pp. 338–345. doi:10.1016/S0022-3093(01)00477-X

[11] Gash, A. E., Satcher, J. H., Jr., Simpson, R. L., and Clapsaddle, B. J., "Nanostructured Energetic Materials with Sol-Gel Methods," *Materials Research Society Symposium Proceedings*, Vol. 800, Materials Research Society, Warrendale, PA, 2003, pp. 55–66.

[12] Prentice, D., Pantoya, M. L., and Clapsaddle. B. J., "Effect of Nanocomposite Synthesis on the Combustion Performance of a Ternary Thermite," *Journal of Physical Chemistry B*, Vol. 109, No. 43, 2005, pp. 20180–20185. doi:10.1021/jp0534481

[13] Subramaniam, S., Hasan, S., Bhattacharya, S., Gao, Y., Apperson, S., Hossain, M., Shende, R. V., Gangopadhyay, S., Redner, P., Kapoor, D., and Nicolich, S., "Self-Assembled Nanoenergetic Composite," *Material Research Society Symposium Proceedings*, Vol. 896, Materials Research Society, Warrendale, PA, 2006, pp. H01-05.1–05.6.

[14] Blobaum, K. J., Reiss, M. E., Plitzko, Lawrence, J. M., and Weihs, T. P., "Deposition and Characterization of a Self-Propagating $CuOx/Al$ Thermite Reaction in a Multilayer Foil Geometry," *Journal of Applied Physics*, Vol. 94, No. 5, 2003, pp. 2915–2922. doi:10.1063/1.1598296

[15] Blobaum, K. J., Wagner, A. J., Plitzko, J. M., Van Heerden, D., Fairbrother, D. H., and Weihs, T. P., "Investigating the Reaction Path and Growth Kinetics in $CuOx/Al$ Multilayer Foils," *Journal of Applied Physics*, Vol. 94, No. 5, 2003, pp. 2923–2928. doi:10.1063/1.1598297

[16] Wang, J., Besnoin, E., Duckham, A., Spey, S. J., Reiss, M. E., Knio, O. M., and Weihs, T. P., "Joining of Stainless-Steel Specimens with Nanostructured Al-Ni Foils," *Journal of Applied Physics*, Vol. 95, No. 1, 2004, pp. 248–256. doi:10.1063/1.1629390

[17] Schoenitz, M., Ward, T., and Dreizin, E. L., "Fully Dense Nano-Composite Energetic Powders Prepared by Arrested Reactive Milling," *Material Research Society Symposium Proceedings*, Vol. 800, Materials Research Society, Warrendale, PA, 2004, pp. AA2.6.1–AA2.6.6.

[18] Schoenitz, M., and Dreizin, E. L., "Nano-Composite Energetic Powders Prepared by Arrested Reactive Milling," U.S. Patent Application No. 10/988,183, filed 12 Nov. 2004.

[19] Schoenitz, M., Ward, T., and Dreizin, E. L., "Fully Dense Nano-Composite Energetic Powders Prepared by Arrested Reactive Milling," *Proceedings of the Combustion Institute*, Vol. 30, 2005, pp. 2071–2078. doi:10.1016/j.proci.2004.08.134

[20] Umbrajkar, S. M., Zhu, X., Schoenitz, M., and Dreizin, E. L., "Effect of Compositional and Structural Refinement on the Ignition and Combustion of Reactive Nanocomposite Powders," *Fourth Joint Meeting of the U.S. Sections of the Combustion Institute*, Combustion Inst., Pittsburgh, PA, 2005, pp. D37/1–D37/6.

[21] Umbrajkar, S. M., Schoenitz, M., and Dreizin, E. L., "Control of Structural Refinement and Composition in $Al–MoO_3$ Nanocomposites Prepared by Arrested Reactive Milling," *Propellants, Explosives, Pyrotechnics*, Vol. 31, No. 5, 2006, pp. 382–389. doi:10.1002/prep.200600052

[22] Takacs, L., "Self Sustaining Reactions Induced by Ball Milling," *Progress in Materials Science*, Vol. 47, No. 4, 2002, pp. 355–414. doi:10.1016/S0079-6425(01)00002-0

[23] Ward, T. S., Trunov, M. A., Schoenitz, M., and Dreizin, E. L., "Experimental Methodology and Heat Transfer Model for Identification of Ignition Kinetics of Powdered Fuels," *International Journal of Heat and Mass Transfer*, Vol. 49, Nos. 25–26, 2006, pp. 4943–4954.

[24] Shoshin, Y. L., Trunov, M. A., Zhu, X., Schoenitz, M., and Dreizin, E. L., "Ignition of Aluminum-Rich Al–Ti Mechanical Alloys in Air," *Combustion and Flame*, Vol. 144, No. 4, 2006, pp. 688–697. doi:10.1016/j.combustflame.2005.08.037

[25] Eapen, B. Z., Hoffmann, V. K., Schoenitz, M., and Dreizin, E. L., "Combustion of Aerosolized Spherical Aluminum Powders and Flakes in Air," *Combustion Science and Technology*, Vol. 176, No. 7, 2004, pp. 1055–1069. doi:10.1080/00102200490426433

[26] Schoenitz, M., Dreizin, E. L., and Shtessel, E., "Constant Volume Explosions of Metallic Mechanical Alloys and Powder Blends," *Journal of Propulsion and Power*, Vol. 19, No. 3, 2003, pp. 405–412.

[27] Trunov, M. A., Hoffmann, V. K., Schoenitz, M., and Dreizin, E. L., "Combustion of Boron-Titanium Nanocomposite Powders in Different Environments," Proceedings of 42nd AIAA/ASME/SAE/ASEE Joint Propulsion Conference and Exhibit, Sacramento CA, AIAA Paper 2006-4809, 6–12 July 2006.

[28] Hertzberg, M., Zlochower, I. A., and Cashdollar, K. L., "Metal Dust Combustion: Explosion Limits, Pressures, and Temperatures," *Symposium (International) on Combustion*, Combustion Inst., Pittsburgh, PA, 1992, pp. 1827–1835.

[29] Cashdollar, K. L., and Chatrathi, K., "Minimum Explosible Dust Concentrations Measured in 20-L and 1-M3 Chambers," *Combustion Science and Technology*, Vol. 87, No. 1–6, 1993, pp. 157–171. doi:10.1080/00102209208947213

[30] Larson, A. C., and Von Dreele, R. B., "General Structure Analysis System (GSAS)," Los Alamos National Lab. Rept. LAUR 86-748, Los Alamos, NM, 2004.

[31] Schuster, J. C., and Ipser, H., "The $Al–Al_8MoO_3$ Section of the Binary System Aluminum-Molybdenum," *Metallurgical Transactions A (Physical Metallurgy and Materials Science)*, Vol. 22 , 1991, pp. 1729–1736. doi:10.1007/BF02646496

[32] Umbrajkar, S. M., Schoenitz, M., and Dreizin, E. L., "Solid State Reduction-Oxidation Reactions: An Example When the Isoconversion Approach Fails," *Thermochimica Acta* (submitted for publication).

[33] Glassman, I., *Combustion*, 3rd ed., Academic Press, San Diego, CA, 1996.